SIMULATION OF DAMAGE EVOLUTION IN A TEXTILE COMPOSITE DOUBLE-CANTILEVER BEAM

D. Mollenhauer[a*], E. Iarve[b], E. Zhou[b], T. Breitzman[a], K. Hoos[b], M. Flores[c],

[a]*U.S. Air Force Research Laboratory, 2941 Hobson Way, Wright-Patterson AFB, Ohio 45433, USA*
[b]*University of Dayton Research Institute, Dayton, Ohio, USA*
[c]*University of Texas at El Paso, El Paso, Texas, USA*
**david.mollenhauer@us.af.mil*

Keywords: Textile Composite, Damage Evolution, Double-Cantilever Beam, Simulation

Abstract
Damage evolution in polymer matrix, textile composite, double-cantilever beam (DCB) specimens was simulated. The focus of the study was to examine the effects of tow nesting on the performance of DCB specimens with a single textile layer per adherend. Two plain-weave textile DCB specimens were examined; one with realistic, but perfectly aligned-warp and aligned-weft tows and one with aligned-warp and nested-weft tows. Damage representations consisted of delamination between tows and matrix and delamination between tows and tows. Additionally, damage in resin-rich regions was modeled either using an X-FEM crack plane or a continuum damage mechanics approach. In each type of specimen, realistic tow morphologies were obtained through a digital-chain simulation of the textile processing.

1. Introduction

Textile composite materials are of great interest to many industries, including aerospace, automotive, and wind energy. They offer designers a wide design space that includes the weave architecture, fiber/matrix materials, and processing methods. Developing material properties for design can be approached from many points of view. Homogenized constitutive behavior can generally be obtained using simplified representations of the tow structure with enough simulation accuracy for preliminary and sometimes detailed design. However, the strength behavior of textile composites is not as amenable to these simplified homogenization techniques. Primarily empirical testing is employed to obtain strength and fracture design values. However, computational insight into strength and damage propagation in these materials is desired.

Accurate damage analysis in textile composites will depend on realistic stress analysis, which, in turn, depends on realistic representations of textile tow geometry, especially with respect to multi-layer textiles that experience tow nesting and compaction effects. This work will detail efforts at obtaining damage evolution simulations of textile composite double-cantilever beams comprised of textile layers that are virtually compacted as in a real textile test specimen. The textile tow morphologies were obtained through simulation of the compaction process using a multi-chain digital element technique that allows the generation of textile morphology for a variety of textile architectures subjected to nesting and compaction

effects [1,2]. The resulting tow morphologies were then inserted into a unique stress analysis methodology allowing the robust analysis of complex textile composites [3]. Damage was limited to matrix damage in the form of delamination between tows and matrix and delamination between tows. Additional matrix damage in resin-rich zones was accounted for via either a specialized X-FEM technique [4,5] or a continuum damage mechanics method [6]. Matrix cracking within tows will be addressed in subsequent efforts.

Two textile DCB morphologies were examined. One DCB textile morphology consisted of 2-layers of plain-weave cloth with the warp and weft tows of each layer perfectly aligned. This specimen also contained a discrete, resin-rich layer between both adherends. The second DCB textile morphology consisted of 2-layers of plain-weave cloth with the warp tows perfectly aligned and the weft tows nested via an offset of ¼ of the tow spacing. These layers were allowed to compact together to produce a nested DCB specimen.

2. Brief Description of Analysis Methods

In the interest of brevity, detailed mathematical descriptions of the modeling methods employed in this effort will be avoided. Instead, only brief descriptions of the techniques will be provided.

2.1. Multi-Chain Digital Element for Textile Tow Morphology

The multi-chain digital element method was used in this work to obtain realistic textile tow morphology [1]. In this methodology, a tow is represented as a number of filaments where each filament is a digital chain. A digital chain is composed of many rod-elements, defined as ‘‘digital elements’’, as shown in Figure 1. Rotational nodes connect rod elements. It is thus able to represent a 1D flexible physical entity with a fixed cross-section, such as a fiber.

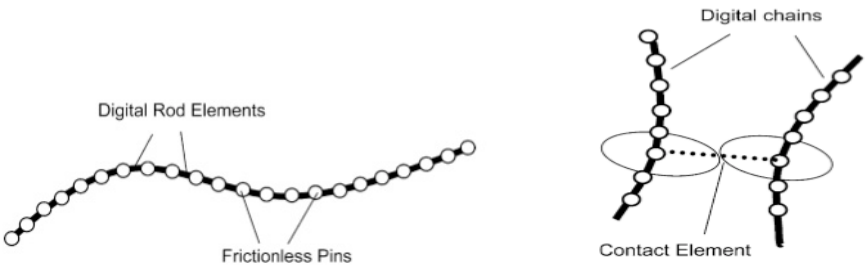

Figure 1: Schematic of a single digital chain (a) and two digital chains (b) interacting through a contact element.

When a digital chain approaches another digital chain, contact between two digital chains can be represented by contact between nodes from two neighboring chains as shown in Figure 1. If the distance between two nodes is smaller than the defined diameter of the digital chain, a contact element is added between them. When contact occurs between two nodes, one of two kinds of physical conditions would exist: sticking or sliding, which is governed by the normal force between nodes and the defined friction coefficients.

Additionally, a vacuum bag or hard mold may be simulated using the multi-chain digital element method. To accomplish this, a network of rod elements are connected via nodes. The stiffness of the vacuum bag is controlled by the stiffness of the rods. A hard mold is enabled by fully constraining the nodes. Figure 2 shows examples of application of the multi-chain digital element method.

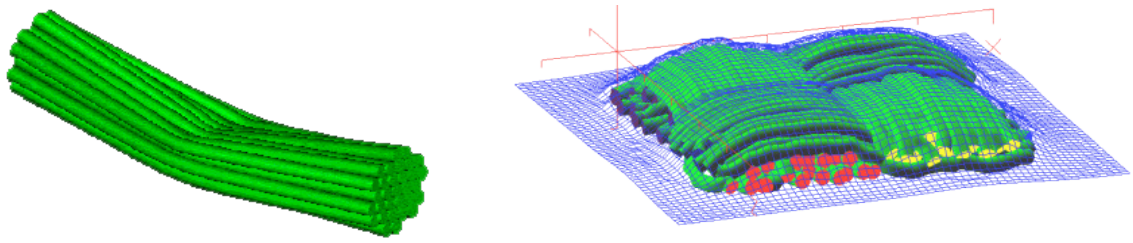

(a) (b)

Figure 2: (a) A single tow represented by multiple digital chains that has been compressed across its middle. (b) A simple plain weave compacted by a digital chain vacuum bag.

2.2. Independent Mesh Method for Textile Stress Analysis

FEM meshes for the textile DCB specimens analyzed in this work were generated from solid representations of the tows obtained from the digital chain simulation method described previously. Once obtained, these tow meshes are combined with an arbitrary mesh representing the matrix, with dimensions equal to the outer dimensions of the specimen. All meshes are developed independently of each other. Much of the matrix mesh occupies space already occupied by the tows. The Independent Mesh Method (IMM) [3] was used for stress analysis of these combined meshes. In the IMM, the shape functions of the matrix displacement approximations are reduced by excluding all functions entirely covered by tows and modifying the integration domain of the shape functions partially covered by tows. The integration is addressed by subdividing the boundary intervals into a total of k^3 integration cubes in the parametric coordinates, as shown in schematically in Figure 3. The integration is carried out by including the contribution of the integration cubes that have at least one node inside the matrix phase. In that respect, we always overestimate the strain energy of the resin. The value of k becomes a solution parameter defining the integration accuracy for the displacement approximation inside the matrix. All connections between contacting fiber tows and fiber and matrix are applied by using a cohesive zone method, allowing for prediction of delamination between tows and matrix and delamination between tows. A k value of 1 was used throughout this research.

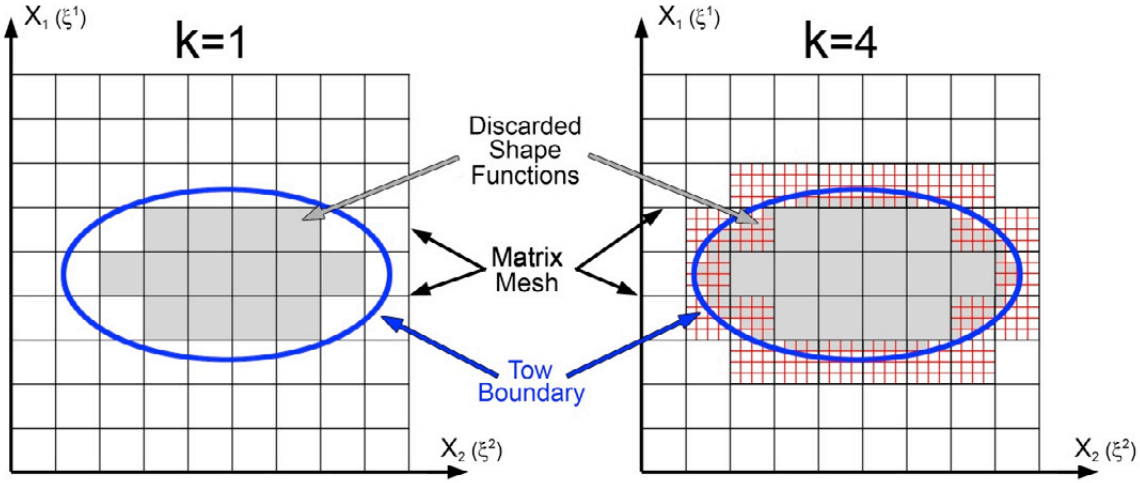

Figure 3: Schematic of matrix displacement approximation function definitions, boundary interval integration, and extra degree of freedom elimination.

2.3. Regularized X-FEM for Matrix Cracking

In this work, one method for simulating matrix damage in resin-rich zones was via a regularized X-FEM (rX-FEM) technique [4,5]. This method allows for the modeling of a displacement discontinuity across a defined surface without the need to remesh the region of interest. In the regularized formulations, the surface of each crack is replaced with a gradient zone and the surface fracture energy with cohesive energy in the gradient zone. The gradient zone is defined by the shape of the smooth approximation of the shape function. In the approach proposed by Iarve [4], the step function is approximated by the same shape functions as the displacements. In this case the Gauss integration points of the initial approximation may be used for integration of the enriched functions.

2.4. Continuum Damage Mechanics Model for Matrix Damage

Another method for accounting for matrix damage in resin-rich zones was via a continuum damage mechanics (CDM) method as described in [6]. The stiffness tensor is defined as $C=(1-d)C_0$, where C_0 is the initial stiffness. Figure 4 describes the proposed response of the matrix, where σ is the maximum principal stress. The damage variable, d, is defined based on the stress strain relationship in Figure 4. Values used for this analysis were $Y_T=77.0\ ^{N}/_{mm2}$, $Y_C=77.0\ ^{N}/_{mm2}$, $G_{YT}=0.177\ ^{N}/_{mm}$, $f_{YT}=0.1$, $f_{GT}=0.6$, where Y_T and Y_C are the matrix strength, G_{YT} is the fracture energy, and F_{YT} and F_{GT} are parameters controlling the shape softening curve. ℓ is the characteristic length of the finite element, which in this case, is calculated from the average element length of 0.05mm across the width of the specimens

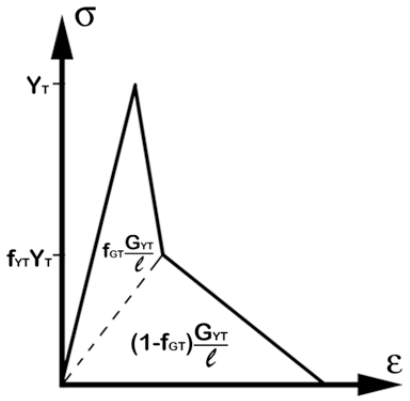

Figure 4: Schematic of the proposed resin uniaxial response in the described in Maimi et al [6].

3. Textile DCB Models

3.1. Virtual Fiber Preform Construction

The multi-chain digital element formulation has been incorporated into a suite of software tools at the Air Force Research Laboratory (AFRL) that is collectively called the Virtual Textile Morphology Suite (VTMS). VTMS was used to produce the initial, idealized fiber paths of a single plain weave preform layer with warp and weft spacing of 1 mm. Fifty-four filaments per tow were added representing approximately 7500 IM7 fibers. The preform was allowed to relax (i.e. filaments redistribute to a natural state accounting for initial filament tension). A virtual vacuum bag was then fitted to the system and allowed to compact the preform against a virtual platen parallel with the XZ-plane. In this manner, a single adherend was created. Selected steps are shown in Figure 5.

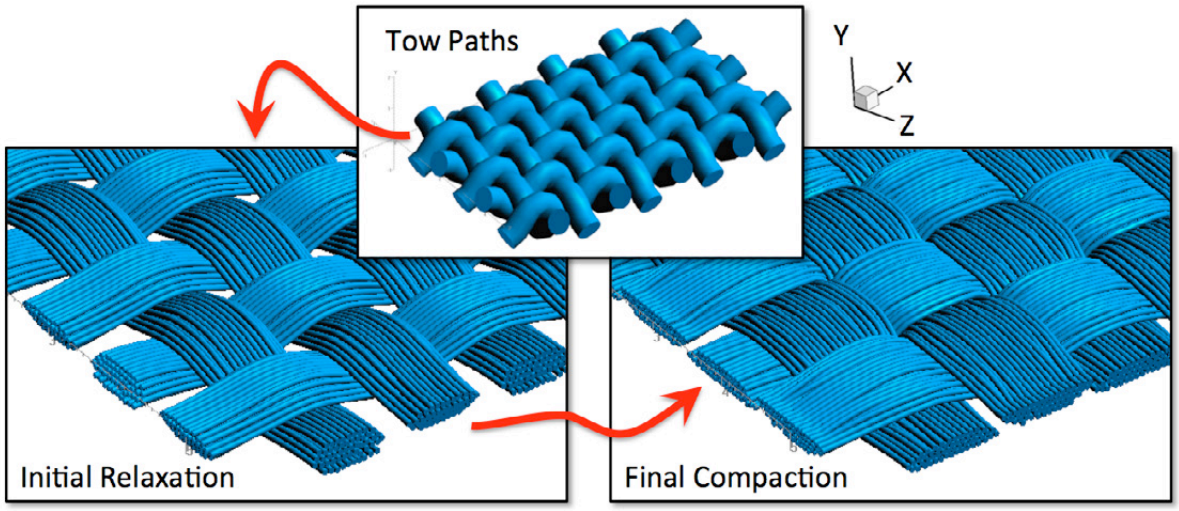

Figure 5: Production of a plain weave layer from tow path generation to initial relaxation to final compaction with a virtual vacuum bag (not shown) and virtual platen (not shown). The warp direction is aligned with X.

This fiber preform was used as a basis for production of the both DCB models. In the aligned-warp, aligned-weft DCB case, two instances of the single preform layer were stacked with the platen sides together and the warp and weft tows aligned. To facilitate a clean fracture plane between the two adherends during damage modeling, a gap of 0.04 mm was intentionally left between the two fiber preform layers. Final preform thickness was approximately 0.75 mm. The aim was to allow both a comparison between the rX-FEM and the CDM approaches for resin-rich region damage evolution as well as the comparison of behavior between an aligned and nested DCB.

The aligned-warp, nested-weft DCB preform was produced in a similar manner. In this case, however, the vacuum bag side of the initial preform was stacked together. The top preform adherend was then shifted by ¼ of a tow spacing (i.e. 0.25 mm) in the X-direction. Two virtual platens (one on the top, one on the bottom) were used to compact the preforms until a preform thickness of 0.75 mm was attained. Before compaction, however, a 0.04 mm thick virtual platen was inserted at Y=0 parallel to the XZ-plane that extended in the X-direction over the first 2 weft tows. This virtual platen served to separate the two adherends in this region and facilitated meshing an initial crack in the subsequent FE solutions. Figure 6 shows a side-view comparison between the two DCB fiber preforms

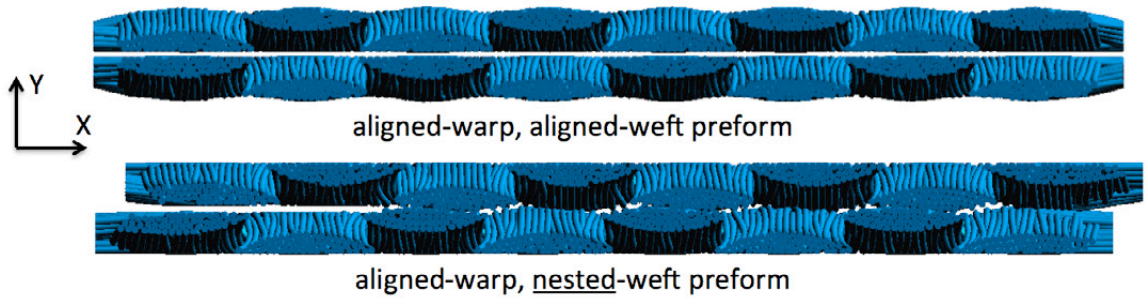

Figure 6: Side-view of both DCB virtual preforms. Note the 0.04 mm gap between adherends in the fully aligned DCB preform and at the left of the nested DCB preform.

3.2. FE Model Details

VTMS was used to extract solid representations of the tows from both DCB virtual preforms in a manner described in [2]. These solid representations were clipped to dimensions of 7 mm in the X-direction and 2 mm in the Z-direction. The resulting solids were meshed with hexahedral solid H-elements within VTMS. A hexahedral H-element mesh for the resin was produced within the open-source meshing code known as Gmsh [7] with dimensions 7 mm in X, 2 mm in Z, and 1.3 mm in Y. The resin mesh included an opening that served as a starter crack with dimensions of 1.5 x 0.04 x 2.0 mm in X, Y, and Z. These meshes were combined in VTMS as shown in Figure 7.

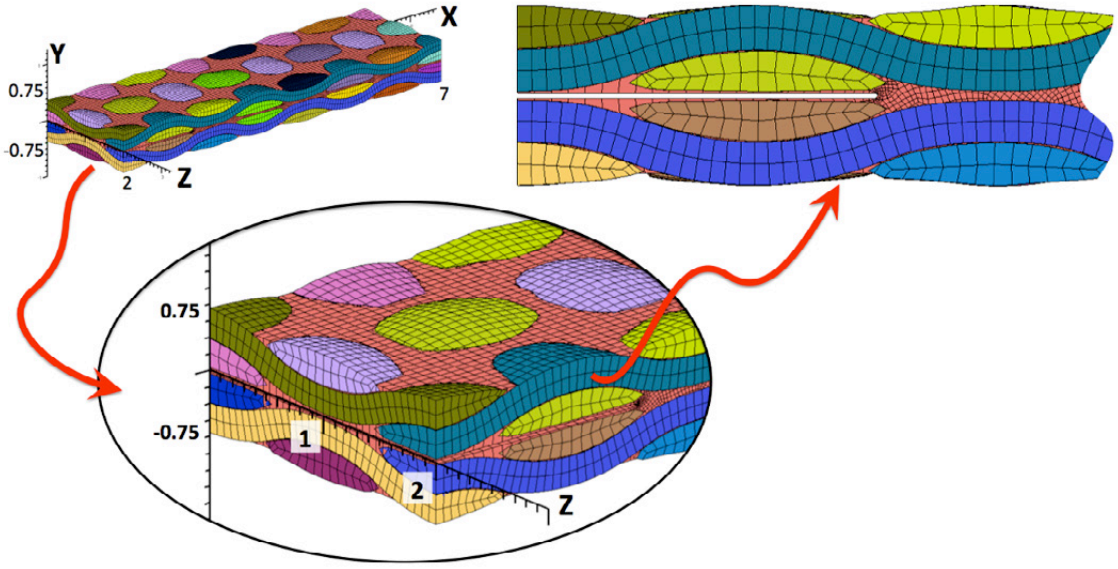

Figure 7: Various views of the combined mesh for the aligned-warp, aligned-weft DCB specimen. Dimensions are in millimeters. For brevity, the aligned-warp, nested-weft mesh is omitted.

Material properties were assigned to the textile tows and matrix pockets according to Table 1. All tows were connected to matrix and to each other via cohesive zone interfaces of the formulation described in [8] with $G_c = 0.177\ ^{N}/_{mm}$ and $Y_t = 77.0\ ^{N}/_{mm2}$. Boundary conditions for both DCB specimens were applied as follows. Incremental displacements were specified at X=0 for the top adherend in the positive Y-direction and in the negative Y-direction for the bottom adherend. At Z=0 and Z=2 mm, $U_z=0$. At X=0, $U_x=0$ at the top corner nodes in the upper adherend and at the bottom corner nodes of the lower adherend.

Property	Composite (IM7/5250-4)	Resin (5250-4)
E_{11} ($^{N}/_{mm2}$)	1.65×10^5	3.45×10^3
E_{22}, E_{33} ($^{N}/_{mm2}$)	1.03×10^4	
G_{13}, G_{12} ($^{N}/_{mm2}$)	5.79×10^3	1.28×10^3
G_{23} ($^{N}/_{mm2}$)	3.31×10^3	
ν_{13}, ν_{12}	0.56	0.35
ν_{23}	0.31	

Table 1: Tow (IM7/5250-4) and resin properties (5250-4) used in the FE modeling of the DCB specimens.

The AFRL FE code known as the B-Spline Analysis Method (BSAM) was used to analyze four separate DCB cases. Two separate damage evolution schemes were used for propagation

of matrix damage in resin pockets between tows and between the two DCB adherends for both the aligned-warp, aligned-weft and the aligned-warp, nested-weft specimens The first scheme involved inserting an rX-FEM cohesive zone, as described in section 2.3, parallel to the XZ-plane at Y=0. The properties used in the cohesive zone were the same as those used for the cohesive zone around each tow. The second scheme employed the continuum damage mechanics model described in section 2.4 with properties of Y_T=77.0 $^N/_{mm2}$, Y_C=77.0 $^N/_{mm2}$, G_{YT}=0.177 $^N/_{mm}$, f_{YT}=0.1, f_{GT}=0.6. Each of the two resin failure schemes were applied to separate models, resulting two separate analyses for each of the textile preform types.

4. Results & Discussion

4.1. Aligned Warp , Aligned Weft DCB Model Results

Load-displacement behavior for the fully aligned DCB specimen for both resin damage propagation methods is shown in Figure 8. Both resin damage propagation schemes appear to agree quite well. Also shown in Figure 8 is a deformed view of the DCB specimen showing the X component of stress and the rX-FEM damage plane. An initially linear portion of the load-displacement curve is followed by a series of load drops and load increases. The location of these features is associated with the location of the resin damage zone with respect to the weft-tow locations. The damage zone approaches the centerline of each weft tow slowly with an accompanying rise in load. As the resin damage passes the centerline of each weft tow, the load rapidly decreases until the damage approaches the next weft tow.

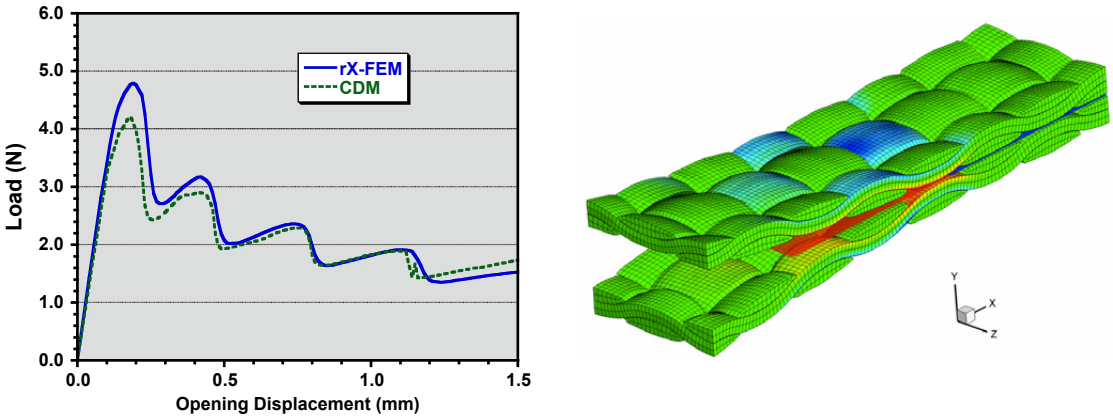

Figure 8: Load-displacement curve from the aligned-warp, aligned-weft DCB model with two forms of resin damage propagation schemes. Deformed X-direction stress with damage plane in red (resin removed for clarity).

4.2. Comparison of Aligned and Nested DCB Model Results

A comparison of load-displacement behavior between aligned and nested DCB specimens is shown in Figure 9. While showing similar trends, the rX-FEM nested prediction is significantly smoother than the rX-FEM aligned prediction, while the CDM nested prediction displays slightly higher loads throughout the loading range. These differences in the nested predictions are believed to be due to the constrained nature of the rX-FEM damage plane. That is, a single plane was defined that allowed the resin to fail only at the midplane of the DCB specimens and at the interfaces between tows. This overly restricts the nature of the failure progression, while the CDM resin propagation failure allows the resin to fail naturally and in concert with the delaminations around the tows. Further efforts with additional nesting configurations and matching experimental efforts will help to understand the differences in prediction techniques.

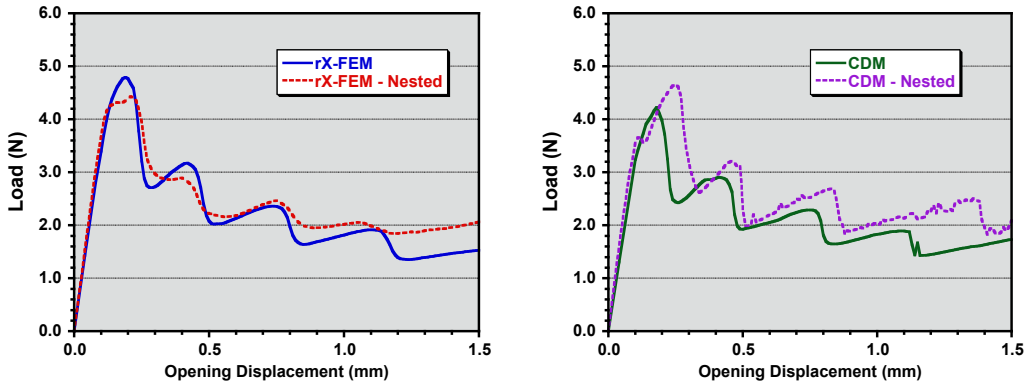

Figure 9: Load-displacement behavior from both DCB specimens with both resin damage propagation schemes.

5. Conclusions

Multiple different techniques were combined to produce numerical model results for 2 textile DCB configurations, an aligned-warp, aligned-weft specimen and an aligned-warp, nested-weft specimen. Realistic tow geometries were obtained using the multi-chain digital element method. Stress analysis was accomplished through the IMM. Delamination around tows was accounted for via a standard cohesive zone method. Finally, resin-rich zone damage was modeled using either an rX-FEM crack plane or a CDM method. Both resin-rich zone damage techniques worked well, especially for the aligned specimen that contained a clean fracture plane between the two adherends. The non-predictive nature of defining an rX-FEM cracking plane, however, may be cause for concern, especially for more complex textile configurations. Reliance on the CDM approach appears to be viable until a self-guided rX-FEM damage propagation scheme can be implemented.

References

[1] G. Zhou, X. Sun, Y. Wang. Multi-chain digital element analysis in textile mechanics. *Composite Science and Technology*, 64:239–244, 2004.

[2] G. Zhou, D. Mollenhauer, E. Iarve. Micro-geometric modeling of textile preforms with vacuum bag compression: an application of multi-chain digital element technique. *Proceedings of the 49th SDM AIAA*, Schaumburg, Illinois, April, 2008.

[3] E.V. Iarve, D.H. Mollenhauer, E.G. Zhou, T.B. Breitzman, and T.J. Whitney. Independent mesh method-based prediction of local and volume average fields in textile composites. *Composites: Part A*, 40:1880-1890, 2009.

[4] E.V. Iarve. Mesh independent modeling of cracks by using higher order shape functions. *International Journal of Numerical Methods in Engineering*, 56:869–882, 2003.

[5] E. Iarve, M. Gurvich, D. Mollenhauer, C. Rose, and C. DaVila. Mesh independent matrix cracking and delamination modeling in laminated composites. *International Journal of Numerical Methods in Engineering*, 2011 (doi: 10.1002/nme.3195).

[6] P. Maimi, P. Camanho, J. Mayugo, C. Davila. A continuum damage model for composite laminates, Part I: *Constitutive model. Mechanics of Materials*, 39:897-908, 2007.

[7] C. Geuzaine and J.-F. Remacle. Gmsh: a three-dimensional finite element mesh generator with built-in pre- and post-processing facilities. *International Journal for Numerical Methods in Engineering*, 79:1309-1331, 2009.

[8] P.P. Camanho, A. Turon, J. Costa, and C.G. Dávila. A damage model for the simulation of delamination in advanced composites under variable-mode loading. *Mechanics of Materials*, 38:1072-1089, 2006.